Research Paper

A Novel Theranostic Combination of Near-infrared Fluorescence Imaging and Laser Irradiation Targeting c-KIT for Gastrointestinal Stromal Tumors

Shota Fujimoto[1], Naoki Muguruma[1], Koichi Okamoto[1], Takeshi Kurihara[1], Yasushi Sato[1], Yoshihiko Miyamoto[1], Shinji Kitamura[1], Hiroshi Miyamoto[1], Takahiro Taguchi[2], Koichi Tsuneyama[3], Tetsuji Takayama[1]✉

1. Department of Gastroenterology and Oncology, Tokushima University Graduate School of Biomedical Sciences, Tokushima, Japan
2. Division of Human Health & Medical Science, Graduate School of Kuroshio Science, Kochi University, Nankoku, Kochi, Japan
3. Department of Pathology and Laboratory Medicine, Tokushima University Graduate School of Biomedical Sciences, Tokushima, Japan

✉ Corresponding author: Tetsuji Takayama, Department of Gastroenterology and Oncology, Tokushima University Graduate School of Biomedical Sciences, 3-18-15, Kuramoto-cho, Tokushima, 770-8503, Japan. Tel: +81-88-633-7124; Fax: +81-88-633-9235; E-mail: takayama@tokushima-u.ac.jp

Abstract

It is difficult to distinguish gastrointestinal stromal tumors (GISTs) from other types of submucosal tumors under conventional gastrointestinal endoscopy. We aimed to detect GISTs by molecular fluorescence imaging using a near-infrared (NIR) photosensitizer (IR700)-conjugated anti-c-KIT antibody and to treat GISTs by photoimmunotherapy with NIR irradiation as a non-invasive theranostic procedure. We also investigated the therapeutic mechanisms.

Methods: Human GIST cell lines GIST-T1 and GIST-882M were incubated with IR700-conjugated anti-c-KIT antibody, IR700-12A8, and observed by confocal laser microscopy. Mice with GIST-T1 xenografts or rats with orthotopic xenografts were injected with IR700-12A8 or AF488-conjugated antibody, and observed under IVIS or autofluorescence imaging (AFI) endoscopy. GIST cells were treated with IR700-12A8 and NIR light *in vitro* and vivo, and cell viability, histology and apoptosis were evaluated.

Results: Strong red fluorescence of IR700-12A8 was observed on the cell membrane of GIST cells and was gradually internalized into the cytoplasm. Tumor-specific accumulation of IR700-12A8 was observed in GIST-T1 xenografts in mice. Under AFI endoscopy, a strong fluorescence signal was observed in orthotopic GIST xenografts in rats through the normal mucosa covering the tumor. The percentage of dead cells significantly increased in a light-dose-dependent manner and both acute necrotic and late apoptotic cell death was observed with annexin/PI staining. Cleaved PARP expression was significantly increased after IR700-12A8-mediated NIR irradiation, which was almost completely reversed by NaN_3. All xenograft tumors (7/7) immediately regressed and 4/7 tumors completely disappeared after IR700-12A8-mediated NIR irradiation. Histologic assessment and TUNEL staining revealed apoptosis in the tumors.

Conclusion: NIR fluorescence imaging using IR700-12A8 and subsequent NIR irradiation could be a very effective theranostic technology for GIST, the underlying mechanism of which appears to involve acute necrosis and supposedly late apoptosis induced by singlet oxygen.

Key words: gastrointestinal stromal tumors (GIST), c-KIT, fluorescence endoscopy, near-infrared photoimmunotherapy

Introduction

Gastrointestinal stromal tumors (GISTs) are the most common submucosal tumors (SMTs) of the alimentary tract [1]. SMTs are derived from mesen- chymal cells and are generally covered with normal mucosa. Accordingly, it is difficult to distinguish GIST from other types of SMTs by conventional

endoscopy. Recently, endoscopic ultrasound-guided fine needle aspiration (EUS-FNA) has been developed to enable histological diagnosis of GIST, but it requires a high degree of technical skill. It is particularly difficult to perform EUS-FNA for small GISTs <2 cm in diameter. Therefore, GISTs <2 cm are merely followed-up periodically without making a histological diagnosis [2]. However, some GISTs <2 cm reportedly show rapid growth and liver metastasis [3,4]. Akahoshi and colleagues reported that 23% of GISTs <2 cm had moderate risk of recurrence according to modified Fletcher classification [5,6]. Therefore, a more simple and effective diagnostic technology is needed for early diagnosis and therapy of GISTs before they develop the potential for malignancy.

Positron emission tomography (PET) is commonly used for the diagnosis of GISTs [7]; however, PET exposes patients to high-dose radiation and it is not specific for GISTs: PET detects not only GIST but also malignant tumors including lymphoma and rhabdomyosarcoma, and even non-malignant inflammatory lesions [8,9]. To provide high specificity for GIST without radiation exposure, fluorescence molecular imaging targeting a specific molecule on tumor cells represents an ideal new technology [10,11]. To date, there has been only one study on fluorescence molecular imaging of GIST involving the targeting of c-KIT, a molecule specifically expressed on GIST cells [12]. In that study, GIST was visualized using Alexa Fluor 488 (AF488)-conjugated anti-c-KIT antibody in a murine GIST model under laparoscopy. However, it yielded a fairly high rate of false-positive signals because of a high degree of autofluorescence in background tissues. Near-infrared (NIR) light is likely to be much more useful for fluorescence imaging because autofluorescence with NIR light is very low [13]. Moreover, NIR light can penetrate tissues much deeper than visible light. Since GISTs are SMTs covered with normal mucosa and more than 90% of GISTs are specifically positive for c-KIT on the cell membrane [14], NIR fluorescence imaging targeting c-KIT appears to be the most suitable strategy for endoscopic molecular imaging of GIST.

Photodynamic therapy (PDT) is a treatment used for several types of cancers, including esophageal cancer, which employs a photosensitizer that is activated by exposure to a specific wavelength of light. The photosensitizer enters cells and its activation causes cell death through production of reactive oxygen species (ROS) [15]. However, these photosensitizers accumulate not only in tumor cells but also in normal tissues, thereby causing severe toxicities [16,17]. Recently, photoimmunotherapy (PIT), using a photosensitizer combined with an antibody against a tumor-specific molecule, has been utilized as a new type of PDT and was reported to show high selectivity [18–20]. However, the use of PIT for GIST has not been reported and the potential underlying biological mechanisms are unknown. In the present study, we first visualized GIST cells using fluorescent NIR photosensitizer-conjugated anti-c-KIT antibodies *in vitro* and *in vivo*. We then evaluated the antitumor activity of PIT, combining a NIR photosensitizer and NIR irradiation, on GIST as a non-invasive theranostic approach. Moreover, we investigated the underlying mechanism of cell death induced by PIT.

Materials and Methods

Cell culture

The human GIST cell lines GIST-T1 and GIST-882M were kindly provided by Dr. Taguchi T (Kochi University, Kochi, Japan) and Dr. Fletcher JA (Brigham and Women's Hospital and Harvard Medical School, Boston, MA), respectively. The GIST-T1 cell line, which has a c-KIT exon 11 heterozygous mutation, was cultured in Dulbecco's modified Eagle medium supplemented with 10% fetal bovine serum (FBS) and 1% penicillin/streptomycin. The GIST-882M cell line, which has a c-KIT exon 13 homozygous mutation, was cultured in Iscove's modified Dulbecco's medium supplemented with 15% FBS, 1% penicillin/streptomycin, and 1% amphotericin B. The human colon cancer cell line SW620 was purchased from ATCC (Manassas, VA) and cultured in RPMI1640 supplemented with 10% FBS. All cells were maintained at 37°C and 5% CO_2 in a humidified incubator.

Synthesis of IR700-conjugated antibodies

Mouse anti-human c-KIT monoclonal antibodies that recognize the extracellular domain of c-KIT, 12A8 (Immuno-Biological Laboratories, Takasaki, Japan), K45 (Thermo Fisher Scientific, Waltham, MA), 104D2 (BioLegend, San Diego, CA), or YB5.B8 (BD Biosciences, San Diego, CA) were used. These antibodies were conjugated with IRDye700 using IRDye® 700DX Protein Labeling Kit (LI-COR Biosciences, Lincoln, NE). Briefly, each anti-c-KIT antibody (100 µg) was incubated with 7 µg of IRDye700DX (IR700) NHS ester in phosphate buffered saline (PBS) containing 100 mM potassium phosphate (pH 8.5) at room temperature for 2 h. The IR700-conjugated antibody was purified using Zeba™ Desalting Spin Columns, 7K MWCO (Thermo Fisher Scientific, Waltham, MA). The protein concentration was calculated from absorbance at 280 nm and 689 nm according to the following formula described in the manufacturer's instructions.

Protein conc. $\left(\dfrac{\text{mg}}{\text{mL}}\right) =$

$$\dfrac{A_{280} - (0.095 \times A_{689})}{\varepsilon_{\text{Protein}}} \times MW_{\text{Protein}} \times \text{dilution factor}$$

The dye per protein ratio was calculated as described previously [21], and was approximately 2.0.

The conjugated antibodies were characterized by non-reducing SDS polyacrylamide gel electrophoresis (SDS-PAGE) and matrix-assisted laser desorption/ionization time-of-flight mass spectrumetry (MALDI-TOF MS) analysis (Fig. S1). The purity of the conjugates was confirmed by fluorescence imaging with a ChemiDoc™ MP Imager (Bio-Rad, Hercules, CA) as well as Coomassie blue staining imaging of non-reducing SDS-PAGE. MALDI-TOF MS analysis with an Autoflex™ speed (Bruker, Billerica, MA) also confirmed the purity of conjugates and appropriate labeling.

In addition, we labeled 12A8 or IR700-12A8 with AF488 to compare the c-KIT affinity of AF488-12A8 and AF488-IR700-12A8, and confirmed that their affinities did not differ, indicating that addition of IR700 to 12A8 antibody does not alter the affinity for c-KIT (Fig. S2).

In vitro cell imaging

For fixed-cell imaging, 1×10^5 cells cultured in 35-mm glass bottom dishes were fixed with 4% paraformaldehyde and blocked with 5% goat serum. The cells were incubated with anti-c-KIT antibodies as the primary antibody (10 µg/mL) at 4°C overnight and were then incubated with goat anti-mouse IgG conjugated with Alexa Fluor 488 (Abcam, Cambridge, UK) as the secondary antibody for 1 h at room temperature, or the cells were incubated with IR700-conjugated mouse anti-c-KIT antibodies (10 µg/mL) at 4°C overnight. After washing with PBS, the samples were mounted with ProLong® Gold Antifade Reagent with DAPI (Thermo Fisher).

For live-cell imaging, the cells were incubated with IR700-conjugated anti-c-KIT antibodies (10 µg/mL) and Hoechst 33342 (Dojindo Laboratories, Kumamoto, Japan) in culture media. After washing with PBS, phenol red-free RPMI1640 medium was added and then fluorescence images were acquired with a Nikon A1R using a 638 nm excitation laser and 700/75-nm band pass emission filter to detect IR700. The fluorescence intensity of individual cells was quantified using Image J software. At least 100 cells were quantified for each cell line and each experiment was repeated 3 times.

In vivo and *ex vivo* fluorescence imaging

All animal experiments were performed according to the guidelines of the Committee on Animal Care and Use of Tokushima University. GIST-T1 or SW620 cells (1×10^7) were implanted in the flanks of 10 athymic BALB/c nude mice (CLEA Japan Inc., Tokyo, Japan). One week after implantation, 100 µg of IR700-12A8 was administered via the tail vein. Fluorescence images were obtained using an IVIS Spectrum (Perkin Elmer Inc., Waltham, MA) with a 675/30 nm excitation filter and a 720/20-nm emission filter. For competition assays, the mice were pre-injected with unlabeled 12A8 (300 µg/mouse) and injected with IR700-12A8 (30 µg/mouse) at 6 h after pre-injection, as described previously [22]. For *ex vivo* imaging, each organ (heart, lung, liver, spleen, kidneys, pancreas and gastrointestinal tract) and tumor were resected from the mice at 120 h after administration of IR700-12A8 (100 µg) and *ex vivo* imaging was performed using the IVIS Spectrum. To quantify the fluorescence intensity, regions of interest (ROIs) with a diameter of 7 mm were selected in each tumor and the background skin, and the fluorescence intensities were calculated using software provided by the manufacturer. The signal to noise (S/N) ratio was calculated as described previously [23].

Fluorescence colonoscopy and *ex vivo* imaging of orthotopic GIST in a rat model

GIST-T1 cells were orthotopically injected into the intestinal tunica muscularis of 4 athymic F344/NJcl-rnu/rnu rats. Four weeks after implantation, the rats received AF488-conjugated anti-c-KIT antibodies, AF488-conjugated non-specific IgG (IgG₁), IR700-conjugated 12A8, or IR700-conjugated non-specific IgG (IgG₁) (2.8 mg/kg, based on our preliminary experiments) via the tail vein. Two days later, the rats underwent laparotomy under anesthesia with ether and the intestine was longitudinally cut open to expose submucosal tumors. The tumors from the rats injected with AF488-conjugated antibodies were observed using a GIF-FQ260Z EVIS LUCERA Gastrointestinal Videoscope (Olympus Co., Tokyo, Japan), which is able to switch between white light and autofluorescence imaging (AFI) modes. The filter set for AFI mode selected blue light for excitation at 390-470 nm, and fluorescence images were obtained through the emission barrier filter at 500-630 nm prior to detection with a charge coupled device (CCD) camera. Tumors from the rats injected with IR700-conjugated antibodies were observed using the IVIS Spectrum. To evaluate the fluorescence intensity, we randomly selected 3 ROIs with a diameter of 1 mm in each tumor and the adjacent background mucosa, and the average fluorescence intensity was quantitated using Image J software.

In vitro NIR laser irradiation

GIST cells (5,000 cells/well) seeded in 96-well plates were incubated with IR700-12A8 (10 μg/mL) for 6 h at 37°C. After washing with PBS, phenol red-free RPMI1640 culture medium was added and the cells were irradiated with 0-100 J/cm² of light at a wavelength of 685 nm using a fiber-pigtailed laser diode (LP685-SF15, Thorlabs Inc., Newton, NJ), as shown in Fig. S3, at a power density of 27.8 mW/cm².

Cell viability assay

Cell viability was accessed by WST-8 assay at 1, 24, and 48 h after irradiation, as described previously [24], and was expressed as the percentage of live cells relative to untreated control cells. For cell death assessment, GIST-T1 cells were incubated with 10 μg/mL of IR700-12A8 at 37°C for 6 h, and the media was replaced with phenol red-free RPMI1640 medium containing 10 mM N-acetyl-L-cysteine (NAC), 10 mM, 30 mM sodium azide (NaN₃), or vehicle. One hour after incubation, the cells were irradiated by NIR laser at a dose of 20 J/cm² or 100 J/cm². Twenty-four hours after irradiation, cell viability was evaluated by WST-8 assay. The percentage of cell death was calculated as 100% minus the percentage of live cells. Some of the treated cells were lysed and subjected to Western blot analysis for cleaved PARP expression.

Annexin V-FITC and propidium iodide (PI) staining assay

Apoptotic and necrotic cell death were assessed by Annexin V-FITC and PI staining using MEBCYTO® Apoptosis Kit (MBL, Nagoya, Japan). Briefly, GIST-T1 cells treated with vehicle alone, IR700-12A8 (10 μg/mL) alone, or IR700-12A8 (10 μg/mL) plus NIR laser (100 J/cm²) were collected at 1, 6, 12, and 24 h after irradiation, washed twice with PBS, and then incubated with Annexin V-FITC and PI in the dark. They were analyzed by flow cytometry using BD FACSVerse (BD Biosciences).

Western blot analysis

Total protein samples were prepared in a lysis buffer (5 mM MgCl₂, 137 mM KCl, 1 mM EDTA, 1 mM EGTA, 1% CHAPS, 10 mM HEPES pH 7.5) containing protease inhibitor cocktail (Sigma Aldrich Japan, Tokyo, Japan). The protein concentration was determined using a Pierce BCA Protein Assay Kit (Thermo Fisher). Equal amounts of proteins were resolved by sodium dodecylsulfate-polyamide gel electrophoresis (SDS-PAGE), and transferred to polyvinylidene fluoride (PVDF) membranes. The membranes were blocked with 5% fat-free dry milk in phosphate buffered saline with Tween (PBS-T) for 1 h, and incubated with the primary antibodies overnight at 4°C. Rabbit anti-human PARP polyclonal antibody (Cell Signaling Technology, Boston, MA), rabbit anti-human Bcl-2 monoclonal antibody (Cell Signaling Technology), or mouse anti-human β-actin monoclonal antibody (Sigma Aldrich) were used as the primary antibodies. The membranes were washed 3 times with PBS-T, and incubated with horseradish peroxidase (HRP)-conjugated anti-rabbit or mouse IgG antibody (GE Healthcare UK Limited, Buckinghamshire, UK) for 1 h at room temperature. The proteins were visualized by chemiluminescence using an ECL detection system (GE Healthcare).

In vivo NIR laser irradiation in mice

Fourteen nude mice implanted with GIST-T1 cells into both the left and right flanks were randomized into 2 groups (7 mice per group); one group was injected with IR700-12A8 and the other with vehicle. IR700-12A8 (100 μg) or vehicle was intravenously injected once a week for 2 weeks. The right-side tumors were irradiated with 100 J/cm²/day of light 3 times weekly after each injection, while the left-side tumors were shaded from light. A total of 4 groups were studied: irradiated right tumors in IR700-12A8-injected mice (IR700-12A8 + laser), non-irradiated left tumors in IR700-12A8-injected mice (IR700-12A8 alone), irradiated right tumors in vehicle-injected mice (NIR laser alone), and non-irradiated left tumors in vehicle-injected mice (vehicle alone), as described in Fig. S4. The tumors were irradiated with 100 J/cm² for 30 min at a power density of 55.5 mW/cm². Tumor volumes were measured as described previously [25]. To assess tumor disappearance, mice were injected intravenously with Alexa Fluor 647-conjugated anti-c-KIT antibodies and fluorescence images were obtained using the IVIS Spectrum.

Histological assessment

Tumors were harvested from mice at days 2, 3, and 4. They were fixed in 10% neutral buffered formalin and embedded in paraffin. Serial sections (3-5 μm) were fixed on glass slides and stained with hematoxylin and eosin (H&E). Apoptotic cells were detected by terminal deoxynucleotidyl transferase-mediated deoxyuridine triphosphate nick-end labeling (TUNEL) staining using an *In situ* Apoptosis Detection Kit (Takara Bio Inc., Shiga, Japan) according to the manufacturer's instructions. The sections were counterstained with Mayer's hematoxylin and TUNEL-positive cells were quantified in 3 randomly selected fields of each section at ×400 magnification.

Immunohistochemistry

Immunohistochemical staining was performed

using the labeled streptavidin-biotin-peroxidase (LSAB) method, as previously described [26]. Briefly, paraffin-embedded sections were deparaffinized in xylene and hydrated in graded ethanol solutions and PBS. Endogenous peroxidase was inactivated by incubation with 0.3% H_2O_2 in methanol. The slides were then heated in 0.01 M citrate buffer (pH = 6.0) at 95°C for 15 min. A rabbit anti-human c-KIT polyclonal antibody (Agilent Technologies, Santa Clara, CA) was used as primary antibody. The sections were incubated with the primary antibody at 4°C overnight, washed with PBS, and incubated with secondary biotinylated antibody (Sigma Aldrich) for 1 h at room temperature. Subsequently, the sections were incubated with streptavidin-HRP conjugate and visualized with DAB chromogen (3',3-diamino-benzidine). Finally, the sections were counterstained with Mayer's hematoxylin.

Statistical analysis

Fluorescence intensities of *in vitro* cell images were compared between IR700-12A8 and IR700-K45 treatment groups using Student's t test. Fluorescence intensities of *in vivo* and *ex vivo* images were compared between the tumors and background using Student's t test. Cell viability, tumor size, and apoptotic index was compared among groups receiving vehicle and IR700-12A8 alone, NIR light alone, or IR700-12A8 plus NIR light using Dunnett's test. The percentage of dead GIST-T1 cells was compared among each of the treatment groups using Dunnett's test. A p-value <0.05 was considered significant.

Results

In vitro GIST cell imaging using IR700-conjugated anti-c-KIT antibodies

We first performed a preliminary study using 4 clones of anti-c-KIT monoclonal antibodies (12A8, K45, 104D2, YB5.B8) that target the extracellular domains of c-KIT [27–30]. We performed immunofluorescence staining on GIST cell lines using each antibody and found that 12A8 and K45 had higher affinity for c-KIT on GIST cells than did 104D2 and YB5.B8 (Fig. S5). We also investigated the inhibitory effect of these antibodies on GIST cell proliferation; however, all the clones exhibited similarly weak growth inhibitory effects on both GIST cell lines (Fig. S6). Therefore, we selected 12A8 and K45 clones in the following experiments.

Considering the c-KIT-specific NIR laser therapy for GIST, we next performed immunofluorescence staining using IRDye700-conjugated 12A8 (IR700-12A8) or K45 (IR700-K45). Representative staining

patterns are shown in Fig. 1A. IR700-12A8 and IR700-K45 showed strong red signals in both GIST-T1 and GIST-882M cells. However, almost no fluorescence signals were observed in SW620 colon cancer cells, which have negligible c-KIT expression [31]. The mean fluorescence intensity with IR700-12A8 in GIST-T1 (49.0 ± 0.5 cps/cell) was significantly higher than with IR700-K45 (47.2 ± 0.6 cps/cell; p<0.05). Likewise, the mean fluorescence intensity with IR700-12A8 in GIST-882M (74.3 ± 0.9 cps/cell) was significantly higher than with IR700-K45 (66.2 ± 1.8 cps/cell; p<0.01) (Fig. 1B). Therefore, we chose to use IR700-12A8 for subsequent GIST imaging experiments, even though difference in fluorescence intensities was not very large.

To observe chronological changes in fluorescence signals from live GIST cells, we pre-incubated GIST-T1 cells with IR700-12A8 at 4°C, and then incubated them at 37°C for 1-6 h. Representative images are shown in Figure 1C. A strong red signal was observed on the cell membrane after pre-incubation (0 h). The signals were then gradually translocated to the cytoplasm at 1 h and 2 h. Almost all signals were translocated inside the cells at 6 h. These results strongly suggest that IR700-12A8 bound to c-KIT on the cell membrane was subsequently internalized into the cells.

In vivo and *ex vivo* GIST cell imaging in a mouse xenograft model

To visualize GIST-xenografted mice with fluorescence molecular imaging, we administered IR700-12A8 into 5 mice implanted with GIST-T1 cells in the flank and observed tumors using the IVIS Spectrum. A representative imaging pattern is shown in Figure 2A. Although NIR fluorescence was observed almost throughout the body at 24 h after injection, it decreased quickly in the background and was confined to the tumor at 48 h. The background signal had further decreased and finally only the tumor was clearly visualized at 120 h. When GIST-xenografted mice were pre-injected with a 10-fold amount of unlabeled 12A8 (300 μg/mouse) followed by IR700-12A8 (30 μg/mouse) for the competition assay, the fluorescence signal in the tumor was markedly decreased at all timepoints observed (Fig. S7), suggesting specific interaction of IR700-12A8 with GIST cells. Furthermore, when IR700-12A8 was injected into 5 mice bearing GIST-T1 (right flank) and SW620 (left flank) tumors, no specific signal was detected in SW620 tumors, in contrast with the strong signal in GIST-T1 tumors, indicating that IR700-12A8 bound specifically to c-KIT on GIST-T1 cells (Fig. 2B). Chronological changes in fluorescence intensity in the tumors and background in 5

xenografted mice were evaluated. The mean fluorescence intensity (± SD) in GIST-T1 tumors peaked at 24 h after injection (5886 ± 594 counts/s/cm²/str), then decreased with time, and almost disappeared at 168 h. Similarly, the mean intensity in SW620 tumors and the background peaked at 24 h (4738 ± 531 counts/s/cm²/str and 3601 ± 296 counts/s/cm²/str), then decreased, and almost

disappeared at 120 h. However, the intensities in GIST-T1 tumors were significantly higher at 24-120 h compared with those in SW620 tumors and the background (Fig. 2C). The signal to noise (S/N) ratio of GIST-T1 tumors increased gradually after injection, peaked at 120 h, then subsequently decreased (3.3 ± 0.2; Fig. 2D). However, the ratio of SW620 tumors was 0.8-1.5 and did not increase during observation.
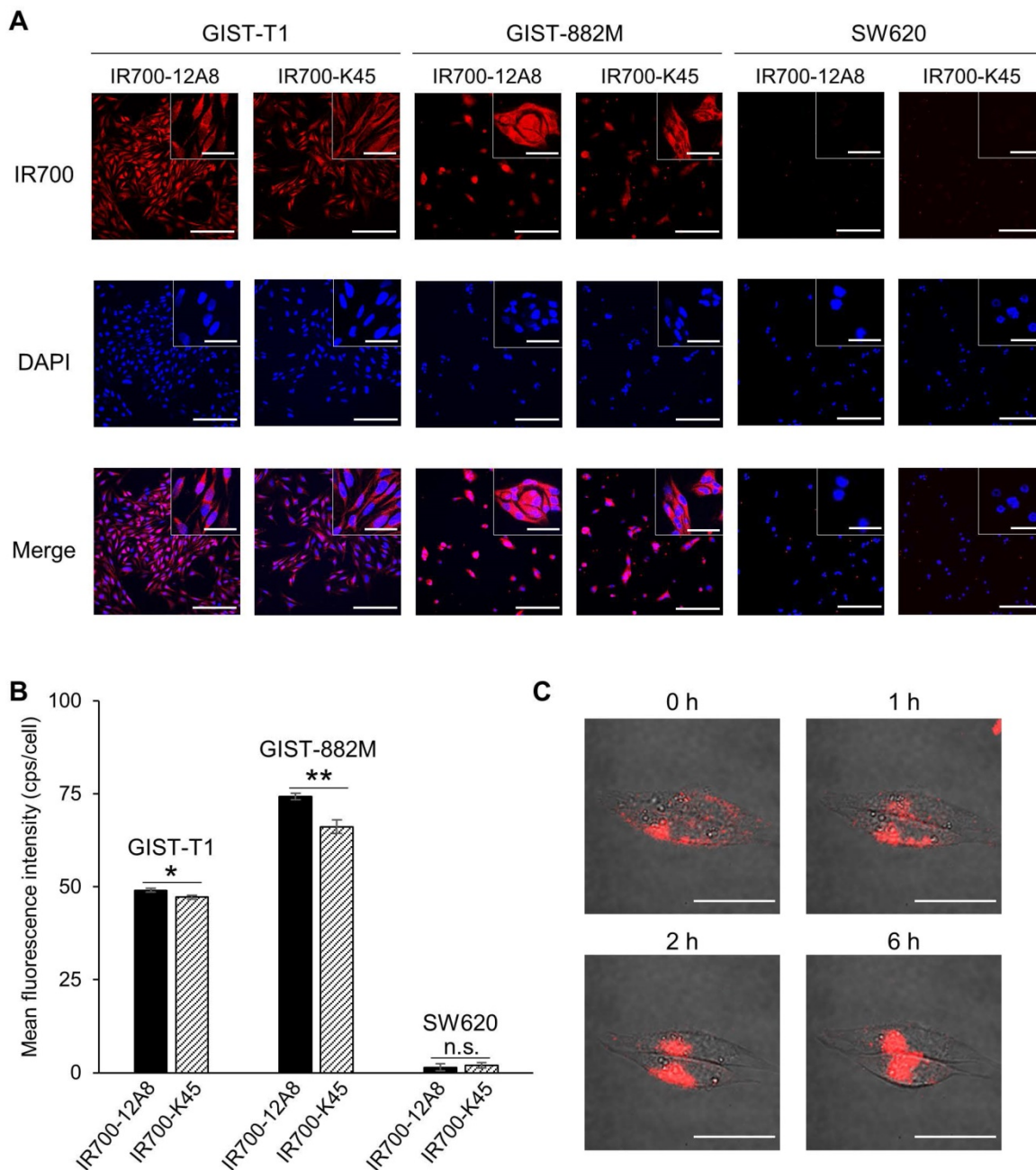

Figure 1. *In vitro* cell imaging of GIST-T1 and GIST-882M cells with IR700-conjugated anti-c-KIT antibodies. (A) Representative staining patterns of GIST-T1 and GIST-882M cells incubated with IR700-conjugated anti-c-KIT antibodies (IR700-12A8 and IR700-K45). Cells fixed with 4% paraformaldehyde were incubated with IR700-conjugated antibody (red) at 4°C overnight. Nuclei were stained with DAPI (blue). SW620 cells were used as a negative control. Original magnification, ×200 (scale bar, 200 μm). High-magnification images are shown in the inset at the upper right (×600) (scale bar, 50 μm). (B) Mean fluorescence intensity in each individual cell. The mean fluorescence intensity of IR700 was quantified using ImageJ software. At least 100 cells were quantified for each cell line and each experiment was repeated 3 times. Data represent mean ± standard deviation (SD) (n.s., not significant; *p<0.05, **p<0.01 by Student's t test). (C) Representative live cell images of GIST-T1 cells with IR700-12A8. The cells were pre-incubated with IR700-12A8 for 6 h at 37°C, and were observed at 0, 1, 2, and 6 h after incubation (scale bar, 50 μm).
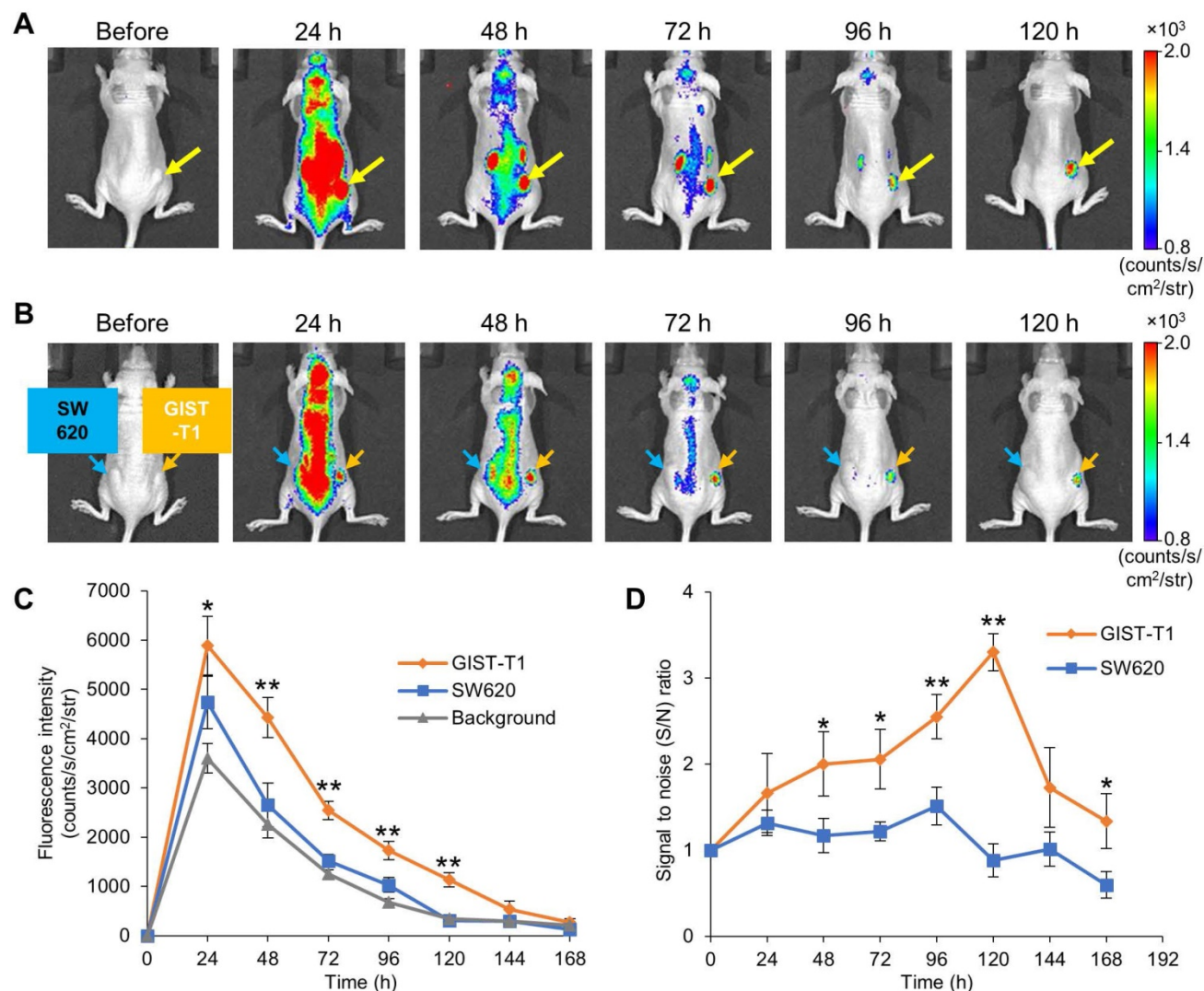
Figure 2. *In vivo* fluorescence imaging of GIST-T1 tumors with IR700-12A8. (A) Representative imaging pattern of GIST-T1 xenograft in mice. IR700-12A8 (100 μg) was intravenously injected into mice with xenografted GIST-T1 cells and fluorescence images were acquired using an IVIS Spectrum. The yellow arrows indicate GIST-T1 tumors. (B) Representative fluorescence images of mice implanted with GIST-T1 cells (right flank, orange arrow) and with SW620 cells (left flank, blue arrow) as a negative control tumor. (C) Chronological changes of the mean IR700 fluorescence intensity in GIST-T1 tumors, SW620 tumors, and background skin. The regions of interest (ROIs) with a diameter of 7 mm were placed in each of the 5 tumors and the opposite side of background skin, and the mean fluorescence intensities were calculated using software provided by the manufacturer. Data represent mean ± SD (n=5; *p<0.05, **p<0.01 by Dunnett's test). (D) Signal to noise (S/N) ratio of IR700 fluorescence in GIST-T1 and SW620 xenograft mice. Data represent mean ± SD (n=5; *p<0.05, **p<0.01 by Student's t test).

The *ex vivo* examination of resected tumors and organs revealed strong fluorescence signals in GIST-T1 tumors (8083 ± 190 counts/s/cm²/str) but weak fluorescence signals in SW620 tumors (2405 ± 484 counts/s/cm²/str), as well as in the liver (1985 ± 119 counts/s/cm²/str) and kidneys (1885 ± 98 counts/s/cm²/str) (Fig. S8).

Endoscopic fluorescence imaging and *ex vivo* imaging in a rat orthotopic GIST model

To visualize orthotopic GIST in nude rats, we implanted GIST cells in the intestinal wall to generate submucosal tumors, administered AF488-conjugated anti-c-KIT antibody or AF488-conjugated non-specific IgG, and observed the tumors using an AFI colonoscope. Representative images are shown in Figure 3A. Typical submucosal tumors, covered with normal mucosa, were identified in the colon 4 weeks after implantation in both rats. When the colons of these rats were opened longitudinally 48 h after injection of AF488-conjugated antibody, similar submucosal tumors were observed with white-light mode under AFI colonoscopy. However, when white-light mode was switched over to AFI mode, a strong green fluorescence signal appeared on the tumor through the normal mucosa covering, although only a low autofluorescence signal was observed in the surrounding background mucosa in a rat treated with AF488-conjugated anti-c-KIT antibody. By contrast, a control rat treated with AF488-conjugated

non-specific IgG showed only a low autofluorescence signal on the tumor, similar to the background signal under AFI. The mean fluorescence intensity in the tumor of the rat treated with AF488-conjugated anti-c-KIT antibody (132.7 ± 8.7 cps/μm^2) was significantly higher than that in the background mucosa (67.0 ± 7.8 cps/μm^2; $p<0.01$) (Fig. 3B), while there was no significant difference in fluorescence intensity between the tumor and the background mucosa in the control rat (71.8 ± 5.4 vs. 67.7 ± 5.2 cps/μm^2).

We subsequently resected the tumors from rats and observed them *ex vivo* using AFI colonoscopy. A strong green fluorescence signal was clearly observed on the tumor of the AF488-antibody-injected rat, whereas only low autofluorescence signal was observed on the tumor of the control rat (Fig. 3A). Both tumors were then pathologically confirmed as GIST based on the characteristic findings of spindle-shaped cells and positivity for c-KIT by immunohistochemistry.
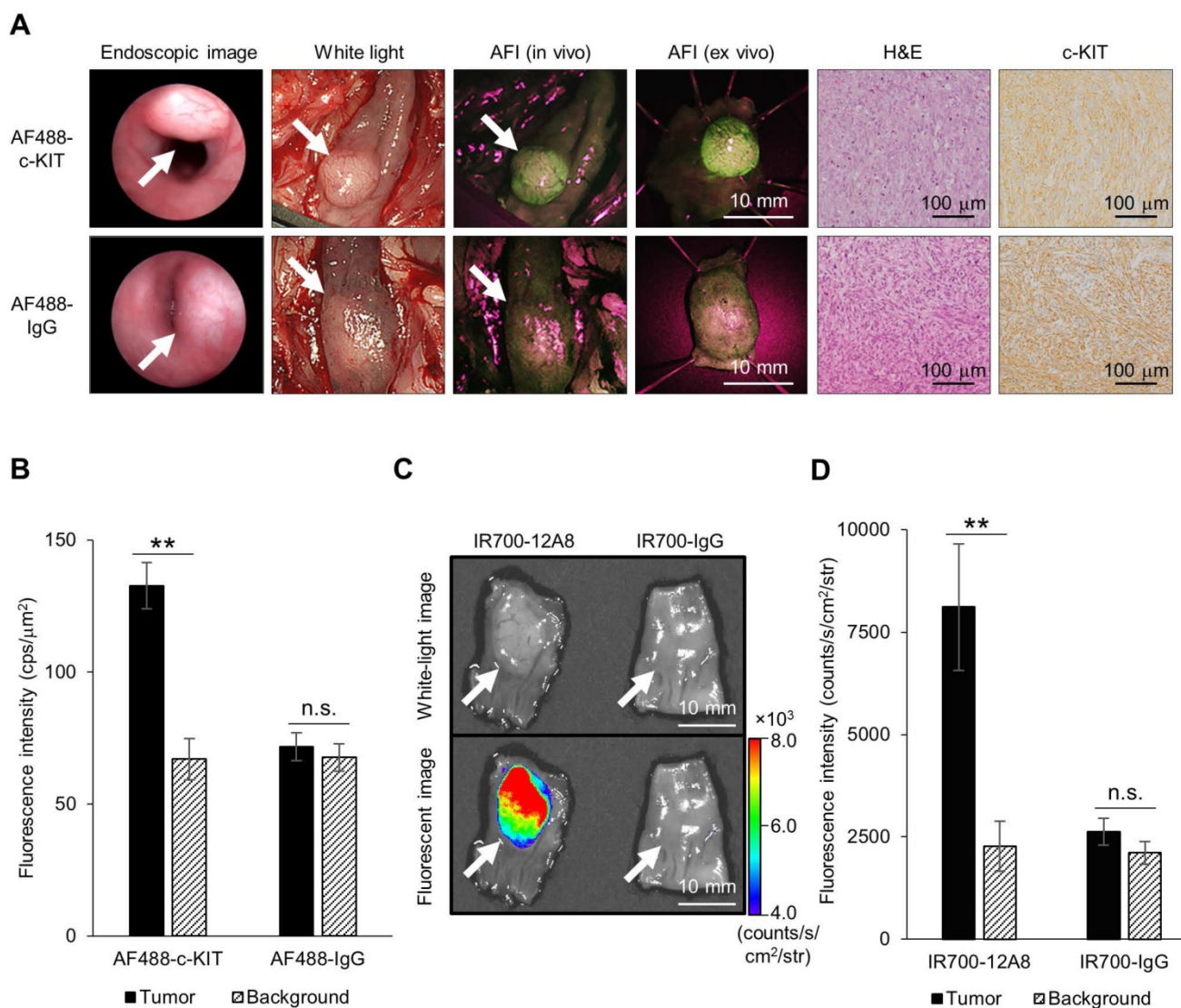

Figure 3. Endoscopic fluorescence imaging and *ex vivo* imaging of orthotopic GIST-T1 tumors in rats using Alexa Fluor 488 (AF488)-conjugated anti-c-KIT antibody or IR700-12A8. (A) Representative endoscopic images of orthotopic GIST-T1 tumors in a rat injected with AF488-conjugated anti-c-KIT antibody (AF488-c-KIT) or AF488-conjugated non-specific IgG (AF488-IgG). The tumors were observed with a veterinary endoscope (endoscopic image), in white light-mode with a human AFI endoscope (white light), in AFI mode with a human AFI endoscope (AFI *in vivo* and *ex vivo*) at 4 weeks after transplantation. White arrows indicate tumors. The tumors were then fixed with formalin, embedded in paraffin, and stained with hematoxylin and eosin (H&E)**,** and immunohistochemistry for c-KIT (c-KIT) was performed (original magnification, ×200). (B) Mean fluorescence intensities of AF488 in orthotopic tumors and background mucosae of the rats. Data represent mean ± SD (n=3; n.s., not significant; **p<0.01 by Student's t test). (C) Representative *ex vivo* white-light and fluorescence images of orthotopic GIST-T1 tumors in a rat injected with IR700-12A8 or IR700-conjugated non-specific IgG (IR700-IgG). The tumors were observed using the IVIS Spectrum. White arrows indicate tumors. (D) Mean fluorescence intensities of IR700 in orthotopic tumors and background mucosae of the rats. Data represent mean ± SD (n=3; n.s., not significant; **p<0.01 by Student's t test).

We also injected rats with IR700-12A8 or IR700-conjugated non-specific IgG (IR700-IgG), excised the tumors, and then observed them *ex vivo* using the IVIS Spectrum. Representative images are shown in Fig. 3C. The rat treated with IR700-12A8 showed strong fluorescence signals specifically on the tumor covered with normal mucosa, while the rat treated with IR700-IgG did not show any tumor-specific fluorescence signals. The mean fluorescence intensity in the tumor of the rat treated with IR700-12A8 (8113 ± 1545 counts/s/cm²/str) was significantly higher than that in the background mucosa (2266 ± 613 counts/s/cm²/str; p<0.01) (Fig. 3D), whereas no significant difference in fluorescence intensity was observed between the tumor and the background mucosa in the rat treated with IR700-IgG (2620 ± 328 vs. 2108 ± 279 counts/s/cm²/str).

Antitumor effect of IR700-12A8-mediated PIT

Since IR700 is known as a photosensitizer, we next treated GIST cells with IR700-12A8 and then irradiated them using a NIR laser to investigate the efficacy of PIT. Treatment with NIR laser alone or IR700-12A8 alone exhibited no effects on GIST-T1 cell viability. When cells treated with IR700-12A8 were irradiated at 10 J/cm², the percentage of cell death was 8% at 1 h after irradiation and increased to 60% at 24 h after irradiation (p<0.01) and then to 78% at 48 h after irradiation (p<0.01). The cell death percentage was increased in a radiation dose-dependent manner, reaching 63% at 1 h and 100% at 24 h and 48 h with irradiation at 100 J/cm² (Fig. 4A).

Since IR700-12A8-mediated PIT showed strong antitumor activity against GIST-T1 *in vitro*, we investigated its *in vivo* effect in GIST-T1-xenografted mice. We first performed *in vivo* experiments using PIT with 50 J/cm² or 100 J/cm² of NIR light based on dosages established from *in vitro* experiments (the detailed treatment schedule is described in Fig. S9A). However, the antitumor effect was limited and the tumors continued to grow, although significant tumor reduction was observed compared with control (Fig. S9). Since no adverse events, including weight loss and cutaneous damage, were observed, we then performed *in vivo* PIT with a higher light dose, i.e., 2 cycles of treatment comprising IR700-12A8 injection and 3 rounds of irradiation at 100 J/cm² (Fig. 4B). To establish the protocol, we checked the intact fluorescence of IR700 in tumors before the first, second, and third 100 J/cm² irradiation (at 24, 48, and 72 h after IR700-12A8 injection) and confirmed that the intact fluorescence of IR700 existed before the second and third irradiation (Fig. S10). Following this regimen, the tumor volume of the control group increased over time and was approximately 4.9 times

larger at day 30 than that at day 0. Similarly, the tumor volumes in mice treated with IR700-12A8 alone or NIR laser alone increased over time and were approximately 5.2 times or 5.9 times larger, respectively, at day 30. In contrast, the tumor volume in mice treated with IR700-12A8-mediated PIT was significantly decreased by 35% soon after treatment in all mice, and the tumors disappeared completely in 4 out of 7 mice thereafter (Fig. 4C and Fig. S11). Fig. 4D shows results from 2 mice that were treated with IR700-12A8 or vehicle and that had 2 xenografts (right and left) at day 30, with irradiation of the right-side tumor and no irradiation of the left-side tumor. The right-side tumor exposed to irradiation alone and the left-side tumor treated with IR700-12A8 alone did not show any regression and both exhibited strong fluorescence signals. However, the right-side tumor treated with both IR700-12A8 and irradiation showed marked regression, and it exhibited no fluorescence signals, suggesting that the tumor disappeared completely. Fig. 4E shows excised tumors from each mouse at day 30. Tumors from mice treated with vehicle alone, NIR laser alone, or IR700-12A8 alone were of comparable size. In contrast, no tumors were observed in 4 mice, and very small tumors (5-6 mm) were observed in 3 mice treated with IR700-12A8-mediated PIT. The respective mean tumor sizes were 10.5 ± 1.0 mm for vehicle alone mice, 10.8 ± 1.1 mm for mice treated with NIR laser alone, and 10.6 ± 2.1 mm for mice treated with IR700-12A8 alone. The mean tumor size of mice treated with IR700-12A8-mediated PIT (2.2 ± 2.7 mm) was significantly smaller than that of the other groups of mice (p<0.01).

Mechanism of IR700-12A8-mediated PIT *in vitro*

To investigate the underlying mechanism of cell death triggered by IR700-12A8-mediated PIT, GIST-T1 cells treated with IR700-12A8-mediated PIT were analyzed by annexin V-FITC and PI staining. When the cells were treated with vehicle alone or IR700-12A8 alone, the percentage of annexin V positive and PI negative (annexin V (+) and PI (-)) or both annexin V and PI positive (annexin V (+) and PI (+)) cells was very low. When the cells were treated with IR700-12A8-mediated PIT, the percentage of annexin V (+) and PI (-) cells was 18%, 24%, 20% and 16% at 1, 6, 12 and 24 h, respectively, after irradiation. Meanwhile, the percentage of annexin V (+) and PI (+) cells was 33%, 35%, 51% and 80% at 1, 6, 12, and 24 h, respectively, after irradiation (Fig. 5A). These results indicate that in about 30% of the treated cells, rapid cell death, such as necrosis, was induced. However, annexin V (+) and PI (-) cells were consistently seen

until 24 h after irradiation and these cells gradually shifted to late apoptotic phase (annexin V (+) and PI (+)), suggesting that late apoptotic cell death also contributed to the mechanism of cell death in our condition.

Therefore, we next assessed apoptosis using GIST-T1 and GIST-882M cells treated with IR700-12A8-mediated PIT by Western blotting for cleaved PARP and Bcl-2. Treatment with IR700-12A8 and NIR irradiation resulted in increased PARP cleavage in both GIST cell lines, while the antiapoptotic factor Bcl-2, which was only expressed in GIST-T1 cells, decreased after treatment (Fig. 5B). To clarify the role of ROS in inducing apoptosis with IR700-12A8-mediated PIT, sodium azide (NaN$_3$), a specific quencher of singlet oxygen, or NAC, a well-known scavenger of ROS, was added to the medium when cells were irradiated with NIR light. Twenty-four hours after irradiation, the percentage of dead cells was significantly decreased in the presence of NaN$_3$ compared with untreated cells (vehicle alone) in a dose-dependent manner, while only partial reduction of phototoxicity was observed in the presence of NAC (Fig. 5C). Furthermore, the expression of cleaved PARP was not increased when the cells were treated with IR700-12A8-mediated PIT in the presence of NaN$_3$ (Fig. 5D). These results indicate that IR700-12A8-mediated PIT induced apoptosis through accumulation of ROS, especially singlet oxygen, in GIST cells.

Apoptosis induced by *in vivo* IR700-12A8-mediated PIT

To assess the *in vivo* relevance of apoptosis following IR700-12A8-mediated PIT, GIST-T1-xenografted mice received IR700-12A8-mediated PIT, and histopathological analysis and TUNEL staining were performed at the timepoints indicated in Fig. 6A. Representative photomicrographs of sections from excised tumors are shown in Fig. 6B. Many apoptotic cells with altered nuclear morphology and chromatin aggregation were observed throughout the tumors from the treatment group. In contrast, many typical spindle-shaped GIST cells and far fewer apoptotic cells were observed in the non-treatment group. TUNEL staining revealed many apoptotic cells in tumors from mice treated with IR700-12A8-mediated PIT at 100, 200, and 300 J/cm^2 (Fig. 6C). The apoptotic index in tumors from mice treated with IR700-12A8 without irradiation was only 3.4%, while it was significantly increased to 28.8%, 57.9%, and 14.7% after irradiation with NIR light at 100, 200, and 300 J/cm^2, respectively (Fig. 6D). These results indicate that IR700-12A8-mediated PIT induced apoptosis in GIST cells in an *in vivo* mouse model, as well as *in vitro*.

Discussion

In this study, we clearly visualized GIST cells *in vitro* and in a mouse xenograft model with high specificity using an NIR photosensitizer-conjugated anti-c-KIT antibody IR700-12A8. We also detected strong fluorescence signals from GIST through the covered normal mucosa under AFI endoscopy in an orthotopically transplanted GIST rat model after injection of fluorophore-conjugated anti-c-KIT antibody. This is the first report of endoscopic fluorescence imaging of GIST. Moreover, PIT in combination with IR700-12A8 and NIR irradiation showed a strong antitumor effect against GIST cells *in vitro* and *in vivo*, resulting in complete disappearance of more than half of all tumors in the xenograft model. Thus, our results raise the possibility that NIR fluorescence imaging targeting c-KIT using IR700-12A8 in combination with NIR irradiation may become an effective theranostic for GIST. Additionally, 2 potential mechanisms of cell death were suggested in our condition of PIT experiments, namely acute necrotic cell death and late apoptotic cell death via production of singlet oxygen.

Generally, conventional PDT using photosensitizers requires protection of the skin and eyes from direct sunlight since the photosensitizers accumulate non-specifically in normal tissue [16,17]. Esophageal cancer patients who are treated with PDT using the photosensitizer talaporfin sodium (Laserphyrin®) are advised to avoid direct sunlight for 2 weeks. However, IR700-conjugated anti-c-KIT antibody does not require sunlight avoidance because it specifically binds to c-KIT in GIST, and c-KIT is not expressed in normal skin and eyes. It is important that IR700-12A8 binds specifically to c-KIT on the cell membrane or is internalized to the cytoplasm of GIST cells for tumor-specific and effective PIT because the half-life of singlet oxygen generated by irradiation is very short (<0.04 μs) and its radius of action is only <0.02 μm [17]. Conversely, the singlet oxygen produced by circulating IR700-12A8 irradiated in the blood of normal tissues causes much less cell damage. In fact, adverse events such as cutaneous damage were not observed after therapy even in the site where the GIST was xenografted. Thus, we surmise that a major advantage of our PIT method for GIST is that it eliminates the need for sunlight avoidance during treatment. In addition, since the quantum yield of IR700 for production of fluorescence is relatively higher (0.44) than that of singlet oxygen (<0.03) [32–34], we are able to minimally irradiate with NIR light for imaging guidance to avoid tissue damage, and to irradiate more strongly for treatment.
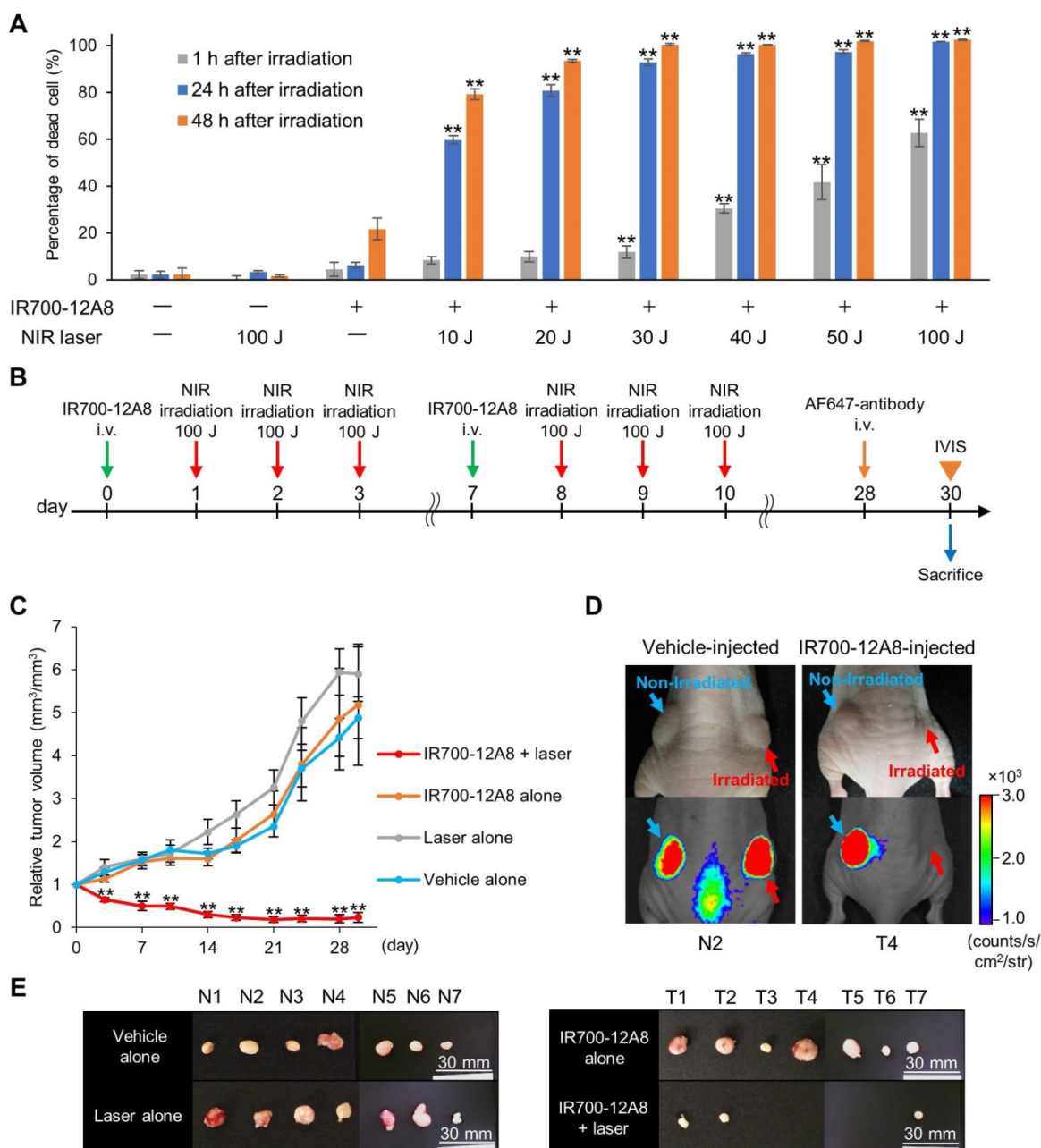
Figure 4. Antitumor effect of IR700-12A8-mediated NIR irradiation. (A) Percentage of dead GIST-T1 cells treated with IR700-12A8 and NIR laser irradiation. Cells were incubated with IR700-12A8 for 6 h at 37°C, and then irradiated with NIR light. Cell viability was assessed by WST-8 assay at 1, 24, or 48 h after irradiation. (n=4; **p <0.01 by Dunnett's test) and the percentage of dead cells was calculated as 100% minus the percentage of live cells. (B) Treatment regimen for *in vivo* IR700-12A8-mediated NIR laser irradiation therapy. Alexa Fluor 647-conjugated anti-c-KIT antibody (AF647-antibody) was injected at day 28 and the tumor was observed using the IVIS Spectrum at day 30, after which the mice were sacrificed for histological analysis. (C) Chronological changes of relative tumor volume in the IR700-12A8 + laser group, IR700-12A8 alone group, laser alone group, and vehicle alone group (n=7 per group). Relative tumor volume (RTV) was calculated using the following formula: RTV = tumor volume at day X / tumor volume at day 0. (**p<0.01 by Dunnett's test) (D) Representative images of vehicle-injected mice (left panel) and IR700-12A8-injected mice (right panel) at day 30. Right-side tumors in each mouse were irradiated, while left-side tumors were not irradiated. White-light images (upper) and fluorescence images (lower) were obtained at 48 h after injection of AF647-antibody. (E) Tumors resected from vehicle-injected group (N1–7) and IR700-12A8-injected group (T1–7) at day 30.

NIR light at wavelengths of 700-1100 nm has much better optical penetration as compared with shorter-wavelength light [35]. Theodore and associates reported that NIR light penetrated up to 30 mm through several types of human soft tissues [36]. Accordingly, NIR light is very suitable for fluorescence-mediated diagnosis and therapy of submucosal lesions such as GIST. Additionally, 4.6% to 46% of initial light at 600-700 nm reportedly remains at a depth of 5-20 mm [37]. Therefore, the entirety of xenograft tumors 6-7 mm in diameter could be easily irradiated by NIR laser, and such tumors appeared to undergo almost complete disappearance. However, it seems that NIR light does

not sufficiently reach distant organs such as liver and kidney through the muscle layer of the gastrointestinal (GI) tract and peritoneum from the mucosal side of the GI tract (stomach, etc.). Moreover, our biodistribution data for IR700-12A8 revealed very low

fluorescence signals in other organs including liver and kidney (Fig. S8). Therefore, damage of these organs by NIR light emitted from the endoscope would likely be minimal.
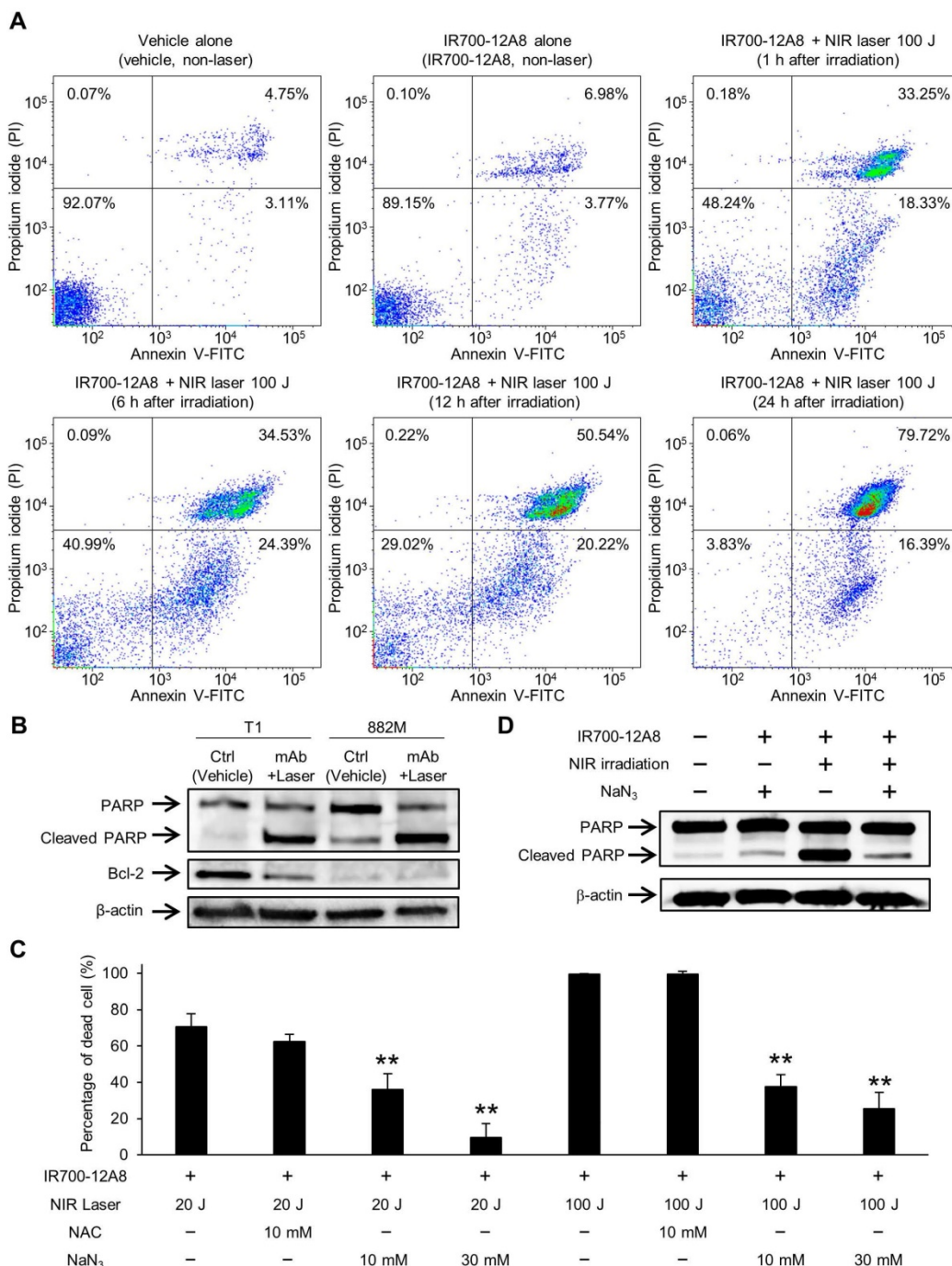

Figure 5. Apoptosis assay and cell death assessment for investigating the therapeutic mechanism of IR700-12A8-mediated NIR irradiation therapy *in vitro*. (A) Annexin V-FITC and propidium iodide (PI) staining of GIST-T1 cells treated with vehicle alone, IR700-12A8 alone, or IR700-12A8 + NIR laser (100 J/cm²). The cells were stained 1, 6, 12, and 24 h after irradiation and were analyzed by flow cytometry. (B) Cleaved PARP and Bcl-2 expression in GIST cells treated with IR700-12A8 and NIR laser irradiation (mAb + Laser). The cells were treated with IR700-12A8 and NIR laser irradiation (20 J/cm²) or vehicle alone (Ctrl), and subjected to Western blot analysis for cleaved PARP and Bcl-2. β-actin was used as a loading control. (C) Cell death evaluation of GIST cells treated with IR700-12A8 and NIR laser irradiation. GIST-T1 cells pre-incubated with IR700-12A8 were incubated with vehicle, N-acetyl-l-cysteine (NAC), or sodium azide (NaN₃) for 1 h, and then were irradiated (20 J/cm² or 100 J/cm²). Cell viability was evaluated 24 h later by WST-8 assay and the percentage of dead cells was calculated as 100% minus the percentage of live cells. Data represent mean ± SD (n=3; **p <0.01 by Dunnett's test). (D) The effect of NaN₃ on the expression of cleaved PARP. GIST-T1 cells treated with vehicle (no treatment), IR700-12A8 and NaN₃, IR700-12A8 and NIR irradiation, or IR700-12A8 and NaN₃ and NIR irradiation were subjected to Western blot analysis.
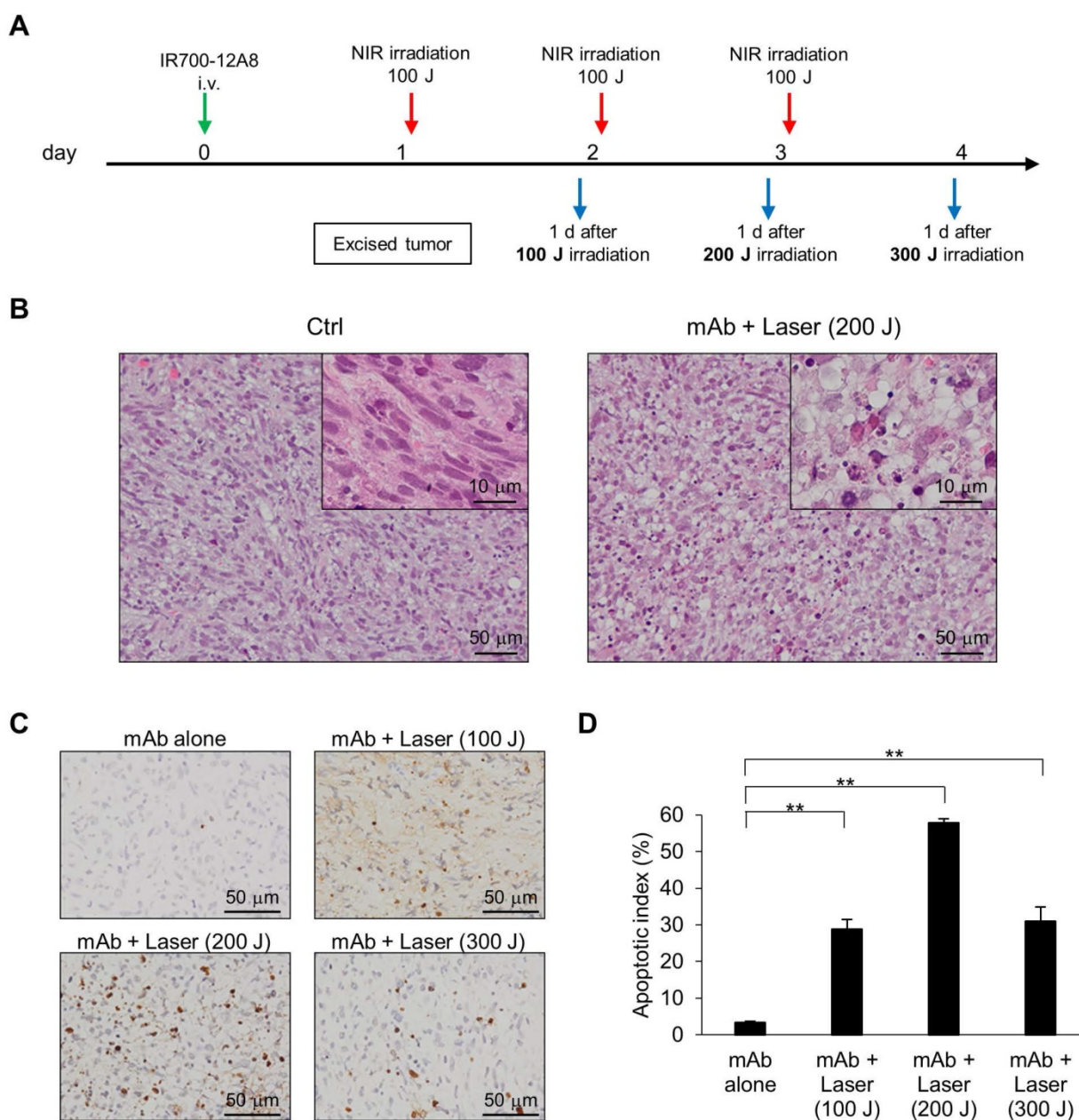
Figure 6. Histological analysis and TUNEL staining of xenografted tumors treated with IR700-12A8-mediated NIR irradiation. (A) Treatment regimen for histological analysis of *in vivo* NIR laser irradiation therapy. (B) Hematoxylin and eosin (H&E) staining of GIST-T1 tumors resected from non-treated mice (Ctrl) and IR700-12A8-mediated NIR irradiated mice (mAb + Laser). Original magnification, ×200. The high-magnification image is shown in the inset (×1000). (C, D) TUNEL staining and apoptotic index of GIST-T1 tumors treated with IR700-12A8 alone (mAb alone) or IR700-12A8-mediated NIR irradiation (mAb + Laser) at 100-300 J/cm². Original magnification, ×400. Apoptotic index was calculated in 3 randomly selected fields of each tumor section. Data represent mean ± SD (n=3; **p <0.01 by Dunnett's test).

In this study, we used a relatively high dose (in Joules) of NIR light irradiation for effective PIT of GIST (10-100 J/cm² on cells and 3×100 J/cm² on tumors) compared with previous studies [38–40]. There are several likely reasons why high-dose irradiation was required in this study. First, the anti-c-KIT antibody (12A8) used in this study induces a rapid internalization of c-KIT receptor to the cytoplasm. Harada and colleagues reported that the internalized fraction of IR700 was less efficient than the cell surface-bound IR700 fraction and had delayed cytotoxic effects probably due to the involvement of more singlet oxygen-dependent apoptotic processes [39]. Thus, we speculate that internalized IR700-12A8 required a higher dose of NIR irradiation. Second, GIST is a sarcoma that is generally more resistant to both radiation and cytotoxic anti-cancer agents as compared with cancer cells. Although no previous studies on PIT for GIST cells have been reported, it is plausible that GIST cells would be more resistant to PIT than other cancer cells.

The therapeutic mechanism of conventional

PDT has been previously reported: when photosensitizer that has accumulated intracellularly is excited by specific light, singlet oxygen is generated, which damages intracellular organelles leading to apoptotic cell death [15]. However, PIT has been reported to induce acute necrotic cell death [18,41]. Furthermore, Mitsunaga and colleagues examined apoptosis in an epidermoid carcinoma cell line (A431) *in vitro* immediately following PIT with IR700-conjugated anti-EGFR antibody and NIR irradiation, but the apoptotic indices were only 5% at 1 h and 18% at 8 h after irradiation, and it was concluded that the mechanism of cell death by PIT does not involve apoptosis [18]. In the present study, we also found that 30-60% of GIST cells underwent early cell death such as necrosis at 1 h after irradiation, but some of the remaining cells slowly underwent apoptosis and then shifted to a late-death fraction in flow cytometry. Regarding apoptosis, PARP cleavage was observed in our *in vitro* PIT experiments and it was suppressed by the singlet oxygen scavenger NaN_3. However, NaN_3 could not completely restore the cells in this study, consistent with previous studies, suggesting that the remaining cell death might be caused by acute cell damage [42,43]. Moreover, with *in vivo* PIT, approximately 30%, 60%, and 30% of cells exhibited apoptosis at 1 day after the first, second, and third 100 J/cm^2 irradiations, respectively, in the TUNEL assay (Fig. 6D). These data demonstrate that IR700-12A8-mediated PIT caused apoptotic cell death, which differs from the findings of Mitsunaga and colleagues, in GIST tumors under our PIT conditions [18]. The antibody used in the present study (IR700-12A8) induced rapid c-kit receptor internalization to the cytoplasm of GIST cells (Fig.1C), which might have contributed to apoptotic cell death in the late phase after PIT, consistent with the findings of Harada and associates [39]. The eventual decrease in the apoptotic index after the third irradiation at 100 J/cm^2 was thought to be due to remaining PIT-resistant tumor cells in the tumor, as well as monoclonal antibody clearance since the half-life of IR700-12A8 after injection was approximately 72 h (Fig. 2C). We also measured temperature changes in cells and xenografted tumors using a thermometer and found that the temperatures in the cells and tumors did not increase during laser therapy (Fig. S12), suggesting that temperature elevation is not an important factor in PIT under our conditions.

Recently, conventional PDT has been reported to activate autophagy in colorectal, breast, and other types of cancers [44,45]. Furthermore, Wei and associates reported that autophagy promotes resistance to apoptosis in colorectal cancer cells [44]. We also examined autophagy activation in GIST cells *in vivo* during PIT using LC3 as a marker and found that LC3 punctate was much more evident in tumors irradiated at 200-300 J/cm^2 (Fig. S13A), and that LC3-II expression was increased at 6, 12, and 24 h after PIT *in vitro* (Fig. S13B), indicating activation of autophagy by IR700-12A8-mediated PIT [46,47]. However, the autophagy inhibitor chloroquine did not significantly affect cleaved PARP expression. These results suggest that autophagy was induced in GISTs by PIT, but apoptotic cell death was not substantially affected by autophagy.

Currently, an AFI endoscope system (500-630 nm; GIF-FQ260Z, Olympus, Co.) is available commercially, while no NIR fluorescence endoscopic system has yet reached this stage of development. We previously developed an infrared fluorescence endoscope to observe cancerous lesions using indocyanine green [48–50]. Slight modification of the observation filter to adjust for the wavelength of IR700 would enable observation of GIST under NIR fluorescence endoscopy with IR700-12A8. Additionally, when whole-body optical fluorescence imaging systems such as IVIS become available, NIR imaging with IR700-12A8 could become a useful method for detecting not only primary GIST lesions but also associated liver or intraperitoneal metastasis. The pharmacokinetics and pharmacodynamics of IR700-12A8, however, require further investigation prior to clinical application. Since 12A8 is a murine anti-c-KIT antibody, humanization of this antibody, which is currently underway, will be needed for clinical use.

In summary, we demonstrated that anti-c-KIT antibody conjugated with the NIR photosensitizer IR700-12A8 provided clear fluorescence imaging of GISTs *in vitro* and *in vivo*. We also clearly visualized GISTs in an orthotopically transplanted rat model through the covered normal mucosa using a fluorophore-conjugated anti-c-KIT antibody under AFI endoscopy. Moreover, IR700-12A8-mediated PIT was very effective for the treatment of GISTs, and the mechanism of this therapeutic effect involved acute necrotic cell death and supposedly late apoptotic cell death via production of singlet oxygen. Thus, our data indicate that IR700-conjugated anti-c-KIT antibodies and NIR irradiation therapy could be a novel effective theranostic technology for GISTs.

Abbreviations

GIST: gastrointestinal stromal tumor; SMT: submucosal tumor; EUS-FNA: endoscopic ultrasound-guided fine needle aspiration; PET: positron emission tomography; NIR: near-infrared; PDT: photodynamic therapy; ROS: reactive oxygen species; PIT: photoimmunotherapy; IR700: IRDye700DX; MALDI-TOF

MS: matrix-assisted laser desorption/ionization time-of-flight mass spectrometry; ROIs: regions of interest; S/N ratio: signal to noise ratio; AFI: autofluorescence imaging; NAC: N-acetyl-L-cysteine; TUNEL: terminal deoxynucleotidyl transferase-mediated deoxyuridine triphosphate nick-end labeling; SD: standard deviation.

Supplementary Material

Supplementary figures.
http://www.thno.org/v08p2313s1.pdf

Competing Interests

The authors have declared that no competing interest exists.

References

1. Hwang JH, Kimmey MB. The incidental upper gastrointestinal subepithelial mass. Gastroenterology. 2004; 126: 301-7.
2. Clinical E, Guidelines P. Gastrointestinal stromal tumours: ESMO Clinical Practice Guidelines for diagnosis, treatment and follow-up. Ann Oncol. 2014; 25: iii21-iii26.
3. Fujita T. Management of small gastrointestinal stromal tumours. Lancet. 2013; 382: 1701.
4. Tanaka J, Oshima T, Hori K, et al. Small gastrointestinal stromal tumor of the stomach showing rapid growth and early metastasis to the liver. Dig Endosc. 2010; 22: 354-6.
5. Joensuu H, Vehtari A, Riihimaki J, et al. Risk of recurrence of gastrointestinal stromal tumour after surgery: an analysis of pooled population-based cohorts. Lancet Oncol. 2012; 13: 265-74.
6. Akahoshi K, Oya M, Koga T, et al. Clinical usefulness of endoscopic ultrasound-guided fine needle aspiration for gastric subepithelial lesions smaller than 2 cm. J Gastrointestin Liver Dis. 2014; 23: 405-12.
7. Demetri GD, von Mehren M, Blanke CD, et al. Efficacy and safety of imatinib mesylate in advanced gastrointestinal stromal tumors. N Engl J Med. 2002; 347: 472-80.
8. Sekiguchi M, Kakugawa Y, Terauchi T, et al. Sensitivity of 2-[18F]fluoro-2-deoxyglucose positron emission tomography for advanced colorectal neoplasms: a large-scale analysis of 7505 asymptomatic screening individuals. J Gastroenterol. 2016; 51: 1122-32.
9. Izumi D, Yoshida N, Watanabe M, et al. Tumor/normal esophagus ratio in (18)F-fluorodeoxyglucose positron emission tomography/computed tomography for response and prognosis stratification after neoadjuvant chemotherapy for esophageal squamous cell carcinoma. J Gastroenterol. 2016; 51: 788-95.
10. Flusberg BA, Cocker ED, Piyawattanametha W, et al. Fiber-optic fluorescence imaging. Nat Methods. 2005; 2: 941-50.
11. Mitsunaga M, Kosaka N, Choyke PL, et al. Fluorescence endoscopic detection of murine colitis-associated colon cancer by topically applied enzymatically rapid-activatable probe. Gut. 2013; 62: 1034-43.
12. Metildi CA, Tang C-M, Kaushal S, et al. *In vivo* fluorescence imaging of gastrointestinal stromal tumors using fluorophore-conjugated anti-KIT antibody. Ann Surg Oncol. 2013; 20: S693-700.
13. Kosaka N, Ogawa M, Choyke PL, et al. Clinical implications of near-infrared fluorescence imaging in cancer. Future Oncol. 2009; 5: 1501-11.
14. Nishida T, Takahashi T, Nakajima K, et al. KIT and PDGFRA mutations of gastrointestinal stromal tumor. J Clin Oncol. 2009; 27: 10560.
15. Castano AP, Demidova TN, Hamblin MR. Mechanisms in photodynamic therapy: part two-cellular signaling, cell metabolism and modes of cell death. Photodiagnosis Photodyn Ther. 2005; 2: 1-23.
16. Orenstein A, Kostenich G, Roitman L, et al. A comparative study of tissue distribution and photodynamic therapy selectivity of chlorin e6, Photofrin II and ALA-induced protoporphyrin IX in a colon carcinoma model. Br J Cancer. 1996; 73: 937-44.
17. Dolmans DE, Fukumura D, Jain RK. Photodynamic therapy for cancer. Nat Rev Cancer. 2003; 3: 380-7.
18. Mitsunaga M, Ogawa M, Kosaka N, et al. Cancer cell–selective *in vivo* near infrared photoimmunotherapy targeting specific membrane molecules. Nat Med. 2011; 17: 1685-91.
19. Jing H, Weidensteiner C, Reichardt W, et al. Imaging and selective elimination of glioblastoma stem cells with theranostic Near-Infrared-Labeled CD133-Specific antibodies. Theranostics. 2016; 6: 862-74.
20. Sato K, Nagaya T, Choyke PL, et al. Near infrared photoimmunotherapy in the treatment of pleural disseminated NSCLC: preclinical experience. Theranostics. 2015; 5: 698-709.
21. Nakajima T, Sano K, Choyke PL, et al. Improving the efficacy of photoimmunotherapy (PIT) using a cocktail of antibody conjugates in a multiple antigen tumor model. Theranostics. 2013; 3: 357-65.
22. Zou P, Xu S, Povoski SP, et al. Near-infrared fluorescence labeled anti-TAG-72 monoclonal antibodies for tumor imaging in colorectal cancer xenograft mice. Mol Pharm. 2009; 6: 428-40.
23. Muguruma N, Okamoto K, Nakagawa T, et al. Molecular imaging of aberrant crypt foci in the human colon targeting glutathione S-transferase P1-1. Sci Rep. 2017; 7: 6536.
24. Tanaka M, Kataoka H, Yano S, et al. Antitumor effects in gastrointestinal stromal tumors using photodynamic therapy with a novel glucose-conjugated chlorin. Mol Cancer Ther. 2014; 13: 767-75.
25. Sato M, Muguruma N, Nakagawa T, et al. High antitumor activity of pladienolide B and its derivative in gastric cancer. Cancer Sci. 2014; 105: 110-6.
26. Inoue A, Okamoto K, Fujino Y, et al. B-RAF mutation and accumulated gene methylation in aberrant crypt foci (ACF), sessile serrated adenoma/polyp (SSA/P) and cancer in SSA/P. Br J Cancer. 2015; 112: 403-12.
27. Yoshida C, Tsuji AB, Sudo H, et al. Therapeutic efficacy of c-kit-targeted radioimmunotherapy using 90Y-labeled anti-c-kit antibodies in a mouse model of small cell lung cancer. PLoS One. 2013; 8: e59248.
28. Ashman LK, Cambareri AC, To LB, et al. Expression of the YB5.B8 antigen (c-kit proto-oncogene product) in normal human bone marrow. Blood. 1991; 78: 30-7.
29. Cruz AC, Frank BT, Edwards ST, et al. Tumor necrosis factor-alpha-converting enzyme controls surface expression of c-Kit and survival of embryonic stem cell-derived mast cells. J Biol Chem. 2004; 279: 5612-20.
30. Blair A, Sutherland HJ. Primitive acute myeloid leukemia cells with long-term proliferative ability *in vitro* and *in vivo* lack surface expression of c-kit (CD117). Exp Hematol. 2000; 28: 660-71.
31. Chen EC, Karl TA, Kalisky T, et al. KIT signaling promotes growth of colon xenograft tumors in mice and is up-regulated in a subset of human colon cancers. Gastroenterology. 2015; 149: 705-17.
32. Tynan CJ, Clarke DT, Coles BC, et al. Multicolour single molecule imaging in cells with near infra-red dyes. PLoS One. 2012; 7: e36265.
33. Lin H, Zhang R, Gunn JR, et al. Comparison of Cherenkov excited fluorescence and phosphorescence molecular sensing from tissue with external beam irradiation. Phys Med Biol. 2016; 61: 3955-68.
34. Kishimoto S, Bernardo M, Saito K, et al. Evaluation of oxygen dependence on *in vitro* and *in vivo* cytotoxicity of photoimmunotherapy using IR-700-antibody conjugates. Free Radic Biol Med. 2015; 85: 24-32.
35. Bashkatov AN, Genina EA, Kochubey VI, et al. Optical properties of human stomach mucosa in the spectral range from 400 to 2000 nm: Prognosis for gastroenterology. Med Laser Appl. 2007; 22: 95-104.
36. Henderson TA, Morries LD. Near-infrared photonic energy penetration: can infrared phototherapy effectively reach the human brain? Neuropsychiatr Dis Treat. 2015; 11: 2191-208.
37. Quirk BJ, Brandal G, Donlon S, et al. Photodynamic therapy (PDT) for malignant brain tumors — Where do we stand ? Photodiagnosis Photodyn Ther. 2015; 12: 530-44.
38. Sato K, Watanabe R, Hanaoka H, et al. Comparative effectiveness of light emitting diodes (LEDs) and Lasers in near infrared photoimmunotherapy. Oncotarget. 2016; 7: 14324-35.
39. Harada T, Nakamura Y, Sato K, et al. Near-infrared photoimmunotherapy with galactosyl serum albumin in a model of diffuse peritoneal disseminated ovarian cancer. Oncotarget. 2016; 7: 79408-16.

40. Nakamura Y, Bernardo M, Nagaya T, et al. MR imaging biomarkers for evaluating therapeutic effects shortly after near infrared photoimmunotherapy. Oncotarget. 2016; 7: 17254-64.

41. Ogawa M, Tomita Y, Nakamura Y, et al. Immunogenic cancer cell death selectively induced by near infrared photoimmunotherapy initiates host tumor immunity. Oncotarget. 2017; 8: 10425-36.

42. Shirasu N, Yamada H, Shibaguchi H, et al. Potent and specific antitumor effect of CEA-targeted photoimmunotherapy. Int J Cancer. 2014; 135: 2697-710.

43. Jin J, Krishnamachary B, Mironchik Y, et al. Phototheranostics of CD44-positive cell populations in triple negative breast cancer. Sci Rep. 2016; 6: 27871.

44. Wei MF, Chen MW, Chen KC, et al. Autophagy promotes resistance to photodynamic therapy-induced apoptosis selectively in colorectal cancer stem-like cells. Autophagy. 2014; 10: 1179-92.

45. Xue L-Y, Chiu S-M, Oleinick NL. Atg7 deficiency increases resistance of MCF-7 human breast cancer cells to photodynamic therapy. Autophagy. 2010; 6: 248-55.

46. Dolores M, Jorge B, Herna C, et al. Aspirin-induced gastrointestinal damage is associated with an inhibition of epithelial cell autophagy. J Gastroenterol. 2016; 51: 691-701.

47. Gupta A, Roy S, Lazar AJF, et al. Autophagy inhibition and antimalarials promote cell death in gastrointestinal stromal tumor (GIST). Proc Natl Acad Sci U S A. 2010; 107: 14333-8.

48. Ito S, Muguruma N, Kusaka Y, et al. Detection of human gastric cancer in resected specimens using a novel infrared fluorescent anti-human carcinoembryonic antigen antibody with an infrared fluorescence endoscope *in vitro*. Endoscopy. 2001; 33: 849-53.

49. Okamoto K, Muguruma N, Kimura T, et al. A novel diagnostic method for evaluation of vascular lesions in the digestive tract using infrared fluorescence endoscopy. Endoscopy. 2005; 37: 52-7.

50. Kimura T, Muguruma N, Ito S, et al. Infrared fluorescence endoscopy for the diagnosis of superficial gastric tumors. Gastrointest Endosc. 2007; 66: 37-43.